Scalable Architecture for Dark Photon Searches: Superconducting-Qubit Proof of Principle

Runqi Kang,[1,2] Qingqin Hu,[1] Xiao Cai,[3] Wenlong Yu,[3] Jingwei Zhou,[1,2,*] Xing Rong,[1,4,5,†] and Jiangfeng Du[4]

[1]*Laboratory of Spin Magnetic Resonance, School of Physical Sciences, Anhui Province Key Laboratory of Scientific Instrument Development and Application, University of Science and Technology of China, Hefei 230026, China*

[2]*Hefei National Laboratory, University of Science and Technology of China, Hefei 230088, China*

[3]*Gusu Laboratory of Materials, Suzhou, China*

[4]*State Key Laboratory of Ocean Sensing and School of Physics, Zhejiang University, Hangzhou 310058, China*

[5]*Institute of Quantum Sensing, Institute of Fundamental and Transdisciplinary Research and Zhejiang Key Laboratory of R&D and Application of Cutting-edge Scientific Instruments, Zhejiang University, Hangzhou 310058, China*

(Received 12 March 2025; revised 2 August 2025; accepted 7 October 2025; published 29 October 2025)

The dark photon is a well-motivated dark matter candidate that appears in many extensions of the standard model. A fundamental mass-range-sensitivity dilemma is always haunting the dark photon search experiments: resonant haloscopes have excellent sensitivity but are narrowband, while nonresonant haloscopes are broadband but not as sensitive as the resonant ones. A scalable architecture integrating numerous resonant haloscopes would be a desirable solution to this dilemma. However, even the concept of a scalable search remains rarely explored due to the size limitation of conventional haloscopes imposed by the dark photon wavelength. Here, we propose and demonstrate a novel architecture using superconducting qubits as subwavelength haloscope units. By virtue of the scalability of superconducting qubits, it is possible to integrate multiple qubits with different frequencies on a chip-scale device. Furthermore, the frequencies of the qubits can be tuned to extend the search mass range. Thus, our scalable architectures allow for sweepable high-sensitivity dark photon searches at multiple frequencies simultaneously. As a proof-of-principle experiment, we designed and fabricated a three-qubit chip and successfully demonstrated a scalable dark-photon search. Our Letter established constraints on dark photons in the mass range of 15.632–15.638, 15.838–15.845, and 16.463–16.468 μeV, simultaneously, and the constraints are much more stringent than the cosmology constraints. In the future, our Letter can be scaled up to boost the scrutiny of new physics.

DOI: 10.1103/9p1t-vc9j

The hypothetical dark matter shines a light on the ultimate secret of what the Universe is made up of [1–4]. Dark matter also holds great potential to explain many experimental and astronomical anomalies [5–8]. The simplest U(1) gauge boson dark photon is a prime candidate for dark matter. An especially compelling motivation of dark photons comes from the development of theories beyond the standard model, such as string theories and unified field theories. Since many compelling theories assume large symmetry groups, the smallest U(1) symmetry can naturally arise from the decomposition of these high-rank groups [9–13]. Dark photons are predicted to couple very weakly to ordinary matter and have a mass in the range of 10^{-22}–1 eV [14]. Such vast parameter spaces make the experimental search for dark photons a huge challenge.

One of widely utilized techniques for searching for dark photons is the haloscope [14–16]. Projects such as HAYSTAC [17], CAPP [18], QUAX [19,20], ADMX [21], Dark SRF [22], ORGAN [23], and SHANHE [24] use microwave cavities operating at a few gigahertz to conduct resonant detections at μeV scale. The ADMX-Orpheus experiment used a dielectrically loaded cavity working at a higher-order mode for a larger mode volume [25]. The bandwidths of the cavities are usually several hundred kilohertz, depending on the quality factor. In contrast to the resonant haloscopes mentioned above, experiments like FUNK [26], BREAD [27], DOSUE [28], QUALIPHIDE [29], BRASS-p [30], ABRACADABRA [31,32], SHAFT [33], DM-Radio [34], and MADMAX [35] are nonresonant haloscopes, which have larger bandwidths (typically a few gigahertz) at the expense of lower sensitivity. There are also

*Contact author: zhoujw@ustc.edu.cn

†Contact author: xrong@ustc.edu.cn

groups employing superconducting qubits to read out the cavities or tune the frequency of the cavities, such as SQuAD, HAYSTAC, SCaD, and DarQ-Lamb [36–41]. Superconducting qubits have also been proposed as dark matter detectors [42,43]. For the purpose of suppressing thermal noise, most haloscope experiments are carried out in cryogenic systems, such as dilution refrigerators. Given the vast potential parameter space of dark photons, a scalable architecture integrating plentiful resonant haloscopes covering multiple frequencies can be beneficial to the search for dark photons. However, despite intense efforts devoted to the search for dark photons, the scalability of haloscopes remains rarely investigated. Present haloscopes rely on devices with a size comparable to the wavelength of dark photons (on the scale of decimeter), while the limited space in cryogenic systems usually hinders the haloscope devices from scaling up.

Superconducting qubits have emerged as a promising structure for various applications in the booming field of quantum information due to their remarkable scalability [44–46]. Most superconducting qubits operate at a few gigahertz, while their size is typically on the micrometer scale, much smaller than the corresponding wavelength. The small size of superconducting qubits allows integrating a great number of superconducting qubits in a chip-scale device. In this Letter, we describe a novel architecture based on superconducting qubits for experimental dark photon searches. The superconducting qubits are utilized as sensitive dark photon detectors. Each qubit can be driven by a dark photon field with a frequency close to its eigenfrequency. By integrating numerous qubits with various eigenfrequencies, simultaneously searching for dark photons in a wide frequency range can be realized. The search mass range can be further extended by tuning the frequencies of the qubits through magnetic flux. We fabricated a three-qubit chip to demonstrate this proposal. Our experiment successfully shows that the search for dark photon can be conducted with three tunable frequencies simultaneously. Thus, the scalability of the proposal has been verified. Our result established constraints on the kinetic mixing of dark photons in the mass ranges of 15.632–15.638, 15.838–15.845, and 16.463–16.468 μeV, surpassing the constraints from cosmic microwave background distortion by 1 to 2 orders of magnitude.

Our dark-photon-search scheme relies on the kinetic mixing between dark photons and ordinary photons, $\mathcal{L}_{\rm mix} = -(\chi/2)V_{\mu\nu}F_{\mu\nu}$, where χ is the kinetic mixing, $V_{\mu\nu}$ is the ordinary photon field tensor, and $F_{\mu\nu}$ is the dark photon field tensor. Because of the kinetic mixing, a real electric field can be induced by dark photons and then sensed by superconducting qubits [42],

$$E_{\rm X} = \kappa\chi\sqrt{2\rho_{\rm DM}/\epsilon_0}e^{-im_{\rm X}t}, \tag{1}$$

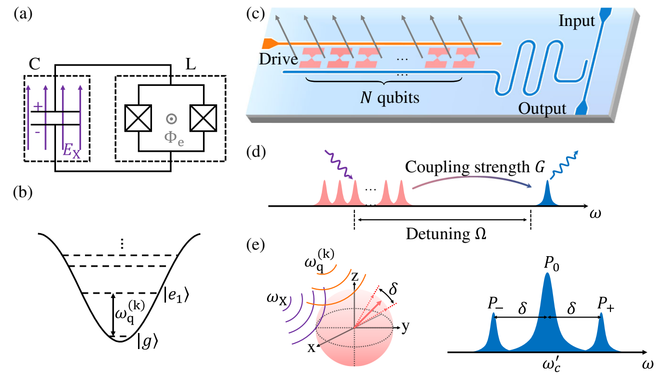

FIG. 1. Dark photon search scheme. (a) Circuit diagram (up) and energy levels (down) of a transmon qubit. The qubit is equivalent to an LC oscillator. The capacitance is sensitive to external electric field (red), while the inductance is sensitive to external magnetic flux (gray). (b) Potential energy and corresponding energy levels for a transmon qubit. The nonlinearity of the oscillator results in a nonquadratic potential (solid line) and unevenly spaced energy levels (dashed lines). (c) Scalable superconductor architecture for dark photon search. It consists of N superconducting transmon qubits (light coral), a readout cavity (blue), and a drive line (orange). The gray arrows refer to the magnetic field for tuning the qubits. (d) Illustration of the concept of many-to-one mapping. All qubits are dispersively coupled to the cavity, so that the output of the cavity contains information at all frequencies of the qubits. (e) Principle of heterodyne detection. The orange curves refer to the artificial driving microwave with frequency $\omega_{\rm q}^{((k)}$ and the purple curves refer to the dark photon field with frequency $\omega_{\rm X}$. There are three peaks in the output of the cavity. The central peak with power P_0 is the reflected probe microwave, while the sideband peaks with the power $P_\pm$ and detuning $\delta = |\omega_{\rm X} - \omega_{\rm q}^{(k)}|$ are the dark-photon-induced signal.

where $\rho_{\rm DM}$ is the local dark matter density [47], ϵ_0 is the vacuum permittivity, $m_{\rm X}$ is the mass of a dark photon, and $\kappa \sim \mathcal{O}(1)$ is the package coefficient introduced by boundary conditions. The concept for a scalable dark photon search is shown in Fig. 1. As Fig. 1(a) shows, each transmon qubit is equivalent to an LC circuit with a capacitance C made of two conductor plates and an inductance L made of two Josephson junctions. The capacitance can accumulate charges in the dark-photon-induced electric field and thus excite the qubit. The two Josephson junctions form a superconducting quantum interference device (SQUID). The inductance L of the SQUID is dependent on the magnetic flux through it, $\Phi_{\rm e}$, so the eigenfrequency of the qubit can be tuned by changing the magnetic flux [45]. The nonlinear nature of Josephson junctions gives rise to a cosine potential energy term and leads to unevenly spaced energy levels, as shown in Fig. 1(b). Consequently, even though a qubit has infinite energy levels, one can regard the qubit as a two-level system with the eigenfrequency $\omega_{\rm q}^{(k)}$, where $k = 1, \ldots N$ is the index of the qubit. The architecture for a scalable dark photon search is illustrated in Fig. 1(c). It contains an array of N superconducting transmon qubits, a resonator, and a drive line. The frequencies of the qubits are tuned through an external magnetic field, as indicated by the gray arrows. Figure 1(d) depicts the concept of the many-to-one mapping from the detecting frequencies to the readout frequency. The eigenfrequencies of the qubits are designed slightly different from each other, forming a comblike structure. The qubits couple to the readout resonator in the dispersive regime, i.e., the detuning $\Omega_{\mathrm{c}}^{(k)} = |\omega_{\mathrm{c}} - \omega_{\mathrm{q}}^{(k)}|$ is larger than the coupling $G^{(k)}$. The Hamiltonian of the interaction between the kth qubit and the cavity is

$$\hat{\mathcal{H}}_{\mathrm{int}}^{(k)} = \hbar g^{(\mathrm{k})} \hat{\tau}_{\mathrm{z}}^{(k)} \hat{a}^{\dagger}\hat{a}, \tag{2}$$

where $\hat{\tau}_{\mathrm{z}}^{(k)}$ is the Pauli operator of the kth qubit, $g^{(k)} = G^{(k)2}/\Omega_{\mathrm{c}}^{(k)}$, and $\hat{a}^{\dagger}$, $\hat{a}$ are the creation and annihilation operators of the cavity [44]. For an arbitrary qubit, the interaction will transduce the change of $\hat{\tau}_{\mathrm{z}}^{(k)}$ into a shift of the resonant frequency of the cavity. In this architecture, each qubit detects the signal resonantly, and the qubit array covers a wide frequency range. Therefore, searching for dark photons at multiple frequencies simultaneously with high sensitivity is feasible.

The heterodyne detection scheme, which is a powerful technology for measuring weak ac signals [48], is applied to each qubit, as shown in Fig. 1(e). The Bloch vector of the qubit, artificially driven by a resonant microwave, deviates from the North Pole of the Bloch sphere and reaches a new equilibrium position, as the solid light coral arrow in Fig. 1(d) shows. For readout, a pure-tone probe microwave of frequency ω_{c}' is injected into the cavity, where ω_{c}' is the frequency at which the absolute slope of the reflection coefficient curve of the cavity, S_{11}, is maximized. The output of the cavity will also be a pure-tone signal with the power P_0. When a dark-photon signal with frequency ω_{X} is sensed by the qubit, the Bloch vector will oscillate around its equilibrium position at frequency $\delta = |\omega_{\mathrm{X}} - \omega_{\mathrm{q}}^{(k)}|$ with amplitude $\boldsymbol{\Delta}\hat{\tau}_{\mathrm{z}}^{(k)}$. Numerically, the amplitude is

$$\boldsymbol{\Delta}\hat{\tau}_{\mathrm{z}}^{(k)} = 1.5\times 10^{-4}\times\kappa\left(\frac{\chi}{10^{-15}}\right)\left(\frac{\omega_{\mathrm{X}}/2\pi}{5\,\mathrm{GHz}}\right)^{\frac{1}{2}}\left(\frac{C}{100\,\mathrm{fF}}\right)^{1/2} \times\left(\frac{d}{300\,\mu\mathrm{m}}\right)\left(\frac{T_1}{50\,\mu\mathrm{s}}\right)^{1/2}\left(\frac{T_2^*}{100\,\mu\mathrm{s}}\right)^{1/2} K(\delta), \tag{3}$$

where d is the distance between the centers of the two conductor plates, T_1 and T_2^* are the longitudinal and transverse relaxation time of the qubit, respectively, and K is a unified line-shape function. In such case, the resonant frequency ω_{c} and reflectivity $S_{11}(\omega_{\mathrm{c}}')$ of the cavity will also oscillate at the frequency δ, and consequently, two additional peaks with the power $P_{\pm} = \boldsymbol{\Delta}P^2/16P_0$ will appear at the sideband of the output spectrum of the cavity, where $\boldsymbol{\Delta}P^2$ is the oscillation amplitude of the output power of the readout cavity,

$$\boldsymbol{\Delta}P = \boldsymbol{\Delta}\hat{\tau}_{\mathrm{z}}^{(k)}\left|\frac{\partial\omega_{\mathrm{c}}}{\partial\hat{\tau}_{\mathrm{z}}^{(k)}}\right|\left|\frac{\partial S_{11}}{\partial\omega_{\mathrm{c}}}\right|\frac{P_0}{S_{11}(\omega_{\mathrm{c}}')}. \tag{4}$$

Their detunings from the main peak are both δ. When the sideband peaks appeared, the bisection method should be used to locate which qubit contributed the signals; while when a null result were obtained, constraints on dark photons at frequencies $\omega_{\mathrm{q}}^{(\mathrm{k})} \pm \delta$ for all values of k could be set simultaneously [see more details in Secs. I and II of Supplemental Material (SM) [49]].

A proof-of-principle experiment searching for dark photons was conducted. The schematic diagram of the experimental apparatus is shown in Fig. 2(a). The entire setup was installed in a multistage cryogenic system. A temperature as low as 14 mK was achieved in the last stage with a dilution refrigerator. Seven input ports were employed. Port $\mathrm{F_k}$ was used to tune the frequency of the kth qubit, Port $\mathrm{D_k}$ were used to drive the kth qubits, and Port C was used to input the probe microwave to the cavity. All the inputs were carefully attenuated so that the input noises were suppressed to a negligible level. It is noteworthy that, in the complete architecture the flux lines can be replaced by a magnet, and all drive lines can be combined with the help of microwave multiplexing. The signal reflected from the cavity was amplified by a cascade of high-electron-mobility transistor amplifiers (HEMTs). The amplified signal was then mixed with a local oscillator signal, down-converted to 1 MHz, and finally acquired by a

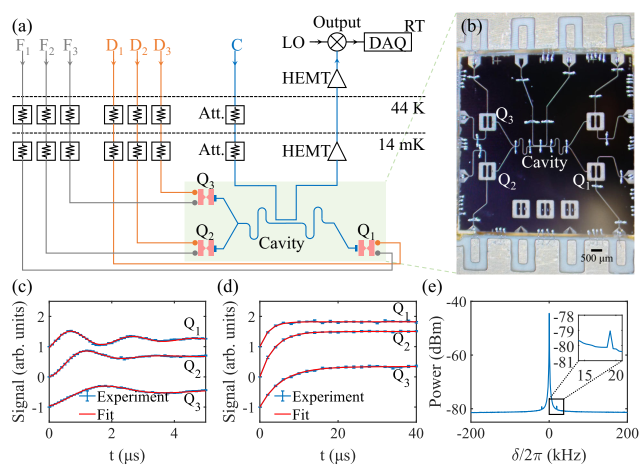

FIG. 2. Experimental system. (a) Schematic diagram of the experimental apparatus. It includes three flux lines ($\mathrm{F_{1,2,3}}$), three drive lines ($\mathrm{D_{1,2,3}}$), a cavity input line (C), an output line, and a three-qubit chip (the green box). (b) Picture of the superconducting qubit chip. (c) Experimental results of Ramsey oscillations of the qubits. (d) Experimental results of T_1 measurements of the qubits. (e) Output spectrum with a simulated dark photon signal.

homemade data acquisition (DAQ) card based on field programmable gate arrays [56,57]. The three-qubit chip is highlighted by the green box in Fig. 2(a) and more details are shown in Fig. 2(b). A 2D cavity and three experimental qubits (Q_1, Q_2, and Q_3) were in the chip. Each experimental qubit is connected to the cavity, a flux line, and a drive line. When the strength of the magnetic flux was set to zero, the initial eigenfrequencies of the qubits were $\omega_{Q1} = 2\pi \times 3780.686$ MHz, $\omega_{Q2} = 2\pi \times 3831.086$ MHz, and $\omega_{Q3} = 2\pi \times 3981.860$ MHz, respectively. The capacitance C and the distance d between two conductor plates were 65 fF and 220 μm for all the qubits. The package coefficient κ was around 3.3, 0.9, and 0.3 for Q_1, Q_2, and Q_3, respectively (see more details in Sec. IV of SM [49]). The resonant frequency of the readout cavity is $\omega_c = 2\pi \times 6595.211$ MHz. Figures 2(c) and 2(d) shows the Ramsey oscillation and the longitudinal relaxation of the qubits. The transverse relaxation time $T_{2,Q_1} = 2.0 \pm 0.1$ μs, $T_{2,Q_2} = 1.1 \pm 0.1$ μs, $T_{2,Q_3} = 1.7 \pm 0.1$ μs, and longitudinal relaxation time $T_{1,Q_1} = 2.3 \pm 0.1$ μs, $T_{1,Q_2} = 3.7 \pm 0.1$ μs, $T_{1,Q_3} = 5.5 \pm 0.2$ μs, are obtained by fitting the data. The detection ability of the system was verified by injecting a pure-tone microwave with a frequency of 3780.669 MHz and a power of 0.1 mW. The injected microwave was a simulation of a dark photon signal with the kinetic mixing $\chi^{\mathrm{sim}} = 6 \times 10^{-12}$. Figure 2(e) shows the output spectrum of the cavity as the blue line. Since the simulated dark photon signal was detuned from ω_{Q1} by $2\pi \times 19$ kHz, there were two sideband peaks at $\delta = \pm 2\pi \times 19$ kHz. The strength and positions of the sideband peaks are consistent with the expectation.

The dark photon search experiment is performed without the simulated dark photon signal. The first dataset contains 60 000 raw spectra, corresponding to an integration time of 9 h. These raw spectra are divided into 150 subsets, each containing 400 raw spectra. Each subset of raw spectra is averaged to suppress the noises. Figure 3(a) shows the average spectrum of Subset 1. Given that the dark photon signals are expected to be symmetric around $\delta = 0$, the two-sided spectrum is converted to a single-sided spectrum in order to improve the signal-to-noise ratio, as Fig. 3(b) shows. Since only the fluctuations rather than the noise itself are concerned, the Savitzky-Golay (SG) filter is applied to remove the baseline of the power spectrum, as the orange lines in Fig. 3(b) shows [58]. Thirty points with strong backgrounds at the center were discarded because the SG filter failed here. The blue dots in Fig. 3(c) depict the standardized power residuals $\Delta_s = (P - P^{\mathrm{SG}})/\sigma$ of Subset 1, where P is the noise power, P^{SG} is the SG filter function, and σ is the standard deviation of the noise power. The gray dots depict the standardized power residuals of Subset 2-150. A standardized power residual exceeding 5 is referred to as a candidate signal. The distribution of the standardized power residuals is illustrated by the red bars in

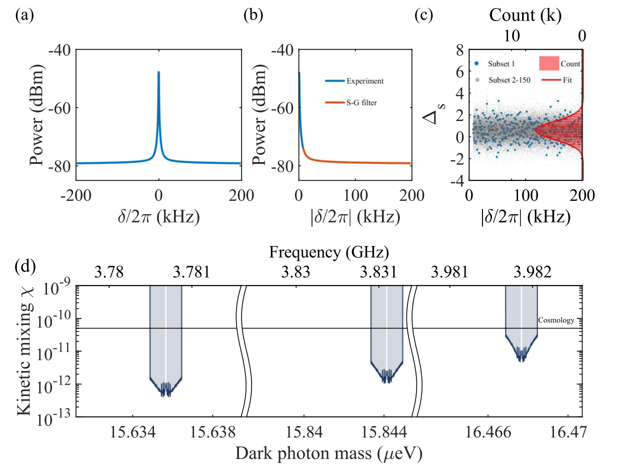

FIG. 3. Results from the first dataset of the experiment. (a) Two-sided spectrum of Subset 1. (b) Single-sided spectrum of Subset 1 and the SG filter. (c) Standardized power residuals and their distribution. (d) Final constraints on dark photons set by this Letter (dark blue) and the cosmology constraints (black) [60].

Fig. 3(c), and the Gaussian fitting result is shown as the red line. No standardized power residual over 5 is observed. Therefore, an exclusion of dark photons can be obtained from experimental results. The data analysis method that gives the upper bound on the kinetic mixing is similar to that developed by ADMX [57,59] (see more details in Sec. V of SM [49]). Figure 3(d) shows the upper bounds on the kinetic mixing with a confidence level of 90%. The left, middle, and right parts of Fig. 3(d) refer to the constraints obtained by considering Q_1, Q_2, and Q_3, respectively. An upper bound of $\chi < 4 \times 10^{-13}$ is achieved at 3780.718 MHz, corresponding to the dark photon mass of 15.636 μeV. This result exceeds the constraints from cosmic microwave background distortions [60] by more than 2 orders of magnitude.

In order to explore more parameter space of dark photons, the eigenfrequencies of the qubits were tuned through a 1 MHz range. The external magnetic flux was generated by injecting dc current from Port F_k. The eigenfrequencies of Q_1, Q_2, and Q_3 swept through the ranges 3780.041–3781.062, 3829.710–3831.086, and 3980.967–3981.860 MHz, respectively, with the current changing from 0 to 29 μA in 17 steps (see more details in Sec. IV of SM [49]). Each tuning was followed by 9-h data

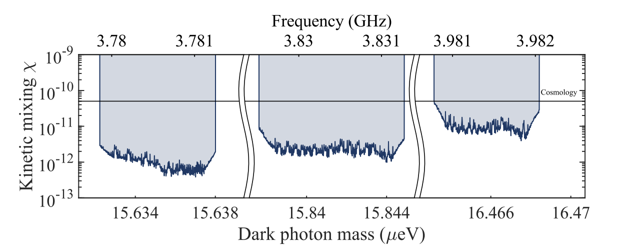

FIG. 4. Combined results from all datasets of the experiment.

TABLE I. Parameters of the detection system.

Configs.	I	II	III	IV	V	VI
$\omega_q/2\pi$ (GHz)	3–5	5–10	10–15	15–20	20–25	25–30
$\varpi_q/2\pi$ (MHz)	1.4	0.3	0.20	0.28	0.40	0.54
$\Delta\omega_q/2\pi$ (MHz)	28	6.0	4.0	5.6	8.0	10.8
Qubit number	72	834	1250	892	625	462

collection, resulting in 17 datasets. The parameter space excluded by all datasets is plotted as the blue regions in Fig. 4. For each qubit, the variation in the exclusions is caused by the degradation of T_2^*, which is resulted from flux noises, and can be avoided using steadier current sources. The results demonstrate the feasibility and practicability of the method proposed in this Letter.

Our Letter opens up the door to scaling up to numerous superconducting qubits on a single chip for scalably searching for dark photons. As listed in Table I, herein we focus on six configurations (ConFigs. I–VI) with lots of qubits evenly distributed in the frequency ranges of several gigahertz, which is shown to be feasible in recent reports [61,62]. Note that although superconducting qubits at 72 GHz have been shown achievable, here we choose a conservative cutoff of 30 GHz [50,51]. The frequency interval between neighboring qubits $\Delta\omega_q$ is designed to be 20 times of the visibility bandwidth of each qubit ϖ_q (see more details in Sec. III of SM [49], and [52,53]). Therefore, with the tuning step being ϖ_q, the targeted frequency range for each configuration can be completely covered within 20 times of tuning. Since the frequency intervals for these configurations are different, the required number of qubits varies from several hundreds to around 1000. For each configuration, the resonant frequency of the readout cavity ω_c is set to be 0.5 GHz lower than the lower bound of the qubit frequency range. For the qubits and the readout cavities, here we choose the conservative values $T_1 = 50$ μs, $T_2^* = 100$ μs, and $Q_{\text{cavity}} = 2\times 10^4 \times (\omega_c/2\pi/1\text{ GHz})^{-2/3}$ considering the yield [25,62–68]. The capacitance C and the distance between two conductor plates d are set to be 100 fF and 300 μm, respectively. The coupling between each qubit and the readout cavity is expected to be $2\pi\times 100$ MHz. The entire setup is housed in a 10 mK dilution refrigerator. The maximum probe power of the cavity is decided by the critical photon number $n_c = \min\{\Omega_c^{(k)2}/4G^2\}$ [44]. The metallic surroundings of the setup is chosen to be a hollow cylinder with the radius R, where $J_0(\omega_c R/c) = 0$, and J_0 is the Bessel function of the first kind. As a result, the package coefficient κ is $1 - J_0(0)/J_0(\omega_q R/c)$. The expected constraints on dark photons are shown as the red lines in Fig. 5 with different shades. For the dashed lines, the integration time is 1 day for every tuning and thus 20 days for the total frequency range, while for the dotted lines, the integration time is 18 days for every tuning and thus 1 yr for the total frequency range, which is practical with techniques suppressing and manipulating potential sources of long-term drifts [66,69,70]. An improvement over the cosmological results of 3 to 5 orders of magnitude is expected. The gray regions in Fig. 5 stand for previous haloscope results.

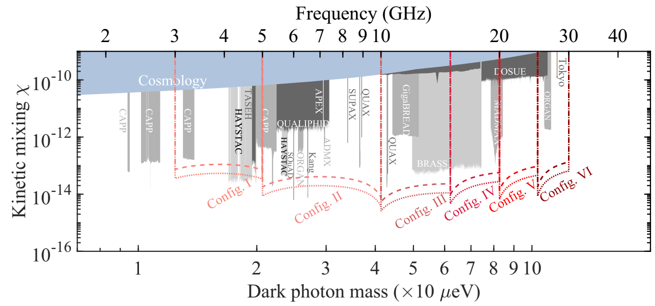

FIG. 5. Expected exclusion limits on the kinetic mixing. The red lines are labeled for their respective configurations. For each configuration, the dashed line and the dotted line indicate the expectation with the integration time of 20 days and 1 yr, respectively. The light blue region stands for the cosmological constraints and the gray regions refer to previous haloscope constraints. Data are adapted from [71].

In conclusion, a scalable architecture for dark photon searches is proposed and experimentally demonstrated in this Letter. The architecture takes advantage of the remarkable scalability of superconducting qubits as well as their sensitive response to the dark-photon-induced electric field, and can enable searching for dark matter with high sensitivity in multiple mass ranges. A proof-of-principle experiment has been successfully realized with a three-qubit chip, and it established the most stringent constraints on dark photons around 15.636, 15.844, and 16.467 μeV, exceeding the previous results by 1 to 2 orders of magnitude. With delicately designed setups, stringent constraints on dark photons can be set in the mass range of 12–66 μeV. This Letter shows that, rather than serving for cavity tuning or readout, superconducting qubits can be directly utilized as detectors for ultralight dark matter, and thus benefit dark matter searches through their scalability. This Letter also lays a foundation for future multifrequency dark matter exploration as qubit number increases and qubit quality continues to be improved.

Acknowledgments—This work was supported by NSFC (Grants No. T2388102, No. 12150010, No. 12205290, No. 12261160569), the Innovation Program for Quantum Science and Technology (2021ZD0302200), the National Key R&D Program of China (Grant No. 2021YFB3202800). X. R. thanks the support by the Major Frontier Research Project of the University of Science and Technology of China (Grant No. LS9990000002). This work was partially carried out at the USTC Center for Micro and Nanoscale Research and Fabrication.

R. K. and Q. H. contributed equally to this work.

Data availability—The data that support the findings of this article are not publicly available. The data are available from the authors upon reasonable request.

[1] H. Poincare, The milky way and the theory of gases, Popular Astron. **14**, 475 (1906).
[2] V. Trimble, Existence and nature of dark matter in the Universe, Annu. Rev. Astron. Astrophys. **25**, 425 (1987).
[3] J. L. Feng, Dark matter candidates from particle physics and methods of detection, Annu. Rev. Astron. Astrophys. **48**, 495 (2010).
[4] G. Bertone and D. Hooper, History of dark matter, Rev. Mod. Phys. **90**, 045002 (2018).
[5] F. Zwicky, The redshift of extragalactic nebulae, Helv. Phys. Acta **6**, 110 (1933).
[6] I. Cholis, L. Goodenough, D. Hooper, M. Simet, and N. Weiner, High energy positrons from annihilating dark matter, Phys. Rev. D **80**, 123511 (2009).
[7] C. Cazzaniga *et al.*, Probing the explanation of the muon (g-2) anomaly and thermal light dark matter with the semi-visible dark photon channel, Eur. Phys. J. C **81**, 959 (2021).
[8] A. W. Thomas and X. G. Wang, Constraints on the dark photon from parity violation and the W mass, Phys. Rev. D **106**, 056017 (2022).
[9] B. Holdom, Two U(1)'s and ϵ charge shifts, Phys. Lett. **166B**, 196 (1986).
[10] B. Holdom, Searching for ϵ charges and a new U(1), Phys. Lett. **178B**, 65 (1986).
[11] M. Goodsell, J. Jaeckel, J. Redondo, and A. Ringwald, Naturally light hidden photons in LARGE volume string compactifications, J. High Energy Phys. 11 (2009) 027.
[12] V. M. Abazov *et al.*, Search for dark photons from supersymmetric hidden valleys, Phys. Rev. Lett. **103**, 081802 (2009).
[13] T. P. Searight, Mirror matter from a unifed field theory, Found. Phys. **51**, 11 (2021).
[14] D. F. J. Kimball and K. van Bibber, *The Search for Ultralight Bosonic Dark Matter* (Springer, Cham, 2023), Chap. 2.
[15] A. Filippi and M. D. Napoli, Searching in the dark: The hunt for the dark photon, Rev. Phys. **5**, 100042 (2020).
[16] A. Caputo, A. J. Millar, C. A. J. O'Hare, and E. Vitagliano, Dark photon limits: A handbook, Phys. Rev. D **104**, 095029 (2021).
[17] B. M. Brubaker *et al.*, First results from a microwave cavity axion search at 24 μeV, Phys. Rev. Lett. **118**, 061302 (2017).
[18] O. Kwon *et al.*, First results from an axion haloscope at CAPP around 10.7 μeV, Phys. Rev. Lett. **126**, 191802 (2021).
[19] D. Alesini *et al.*, Search for invisible axion dark matter of mass $m_a = 43$ μeV with the QUAX-$a\gamma$ experiment, Phys. Rev. D **103**, 102004 (2021).
[20] D. Alesini *et al.*, Search for galactic axions with a high-Q dielectric cavity, Phys. Rev. D **106**, 052007 (2022).
[21] S. J. Asztalos *et al.*, SQUID-based microwave cavity search for dark-matter axions, Phys. Rev. Lett. **104**, 041301 (2010).
[22] A. Romanenko *et al.*, Search for dark photons with superconducting radio frequency cavities, Phys. Rev. Lett. **130**, 261801 (2023).
[23] A. Quiskamp, B. T. McAllister, P. Altin, E. N. Ivanov, M. Goryachev, and M. E. Tobar, Exclusion of axionlike-particle cogenesis dark matter in a mass window above 100 μeV, Phys. Rev. Lett. **132**, 031601 (2024).
[24] Z. Tang *et al.*, First scan search for dark photon dark matter with a tunable superconducting radio-frequency cavity, Phys. Rev. Lett. **133**, 021005 (2024).
[25] R. Cervantes *et al.*, ADMX-Orpheus first search for 70 μeV dark photon dark matter: Detailed design, operations, and analysis, Phys. Rev. D **106**, 102002 (2022).
[26] A. Andrianavalomahefa *et al.*, Limits from the FUNK experiment on the mixing strength of hidden-photon dark matter in the visible and near-ultraviolet wavelength range, Phys. Rev. D **102**, 042001 (2020).
[27] J. Liu *et al.*, Broadband solenoidal haloscope for terahertz axion detection, Phys. Rev. Lett. **128**, 131801 (2022).
[28] S. Kotaka *et al.*, Search for dark photon dark matter in the mass range 74–110 μeV with a cryogenic millimeter-wave receiver, Phys. Rev. Lett. **130**, 071805 (2023).
[29] K. Ramanathan, N. Klimovich, R. B. Thakur, B. H. Eom, H. G. LeDuc, S. Shu, A. D. Beyer, and P. K. Day, Wideband direct detection constraints on hidden photon dark matter with the QUALIPHIDE experiment, Phys. Rev. Lett. **130**, 231001 (2023).
[30] F. Bajjali, S. Dornbusch, M. Ekmedzic, D. Horns, C. Kasemann, A. Lobanov, A. Mkrtchyan, L. H. Nguyen, M. Tluczykont, and G. Tuccari, First results from BRASS-p broadband searches for hidden photon dark matter, J. Cosmol. Astropart. Phys. 08 (2023) 077.
[31] J. L. Ouellet *et al.*, First results from ABRACADABRA-10 cm: A search for sub-μeV axion dark matter, Phys. Rev. Lett. **122**, 121802 (2019).
[32] C. P. Salemi *et al.*, Search for low-mass axion dark matter with ABRACADABRA-10 cm, Phys. Rev. Lett. **127**, 081801 (2021).
[33] A. V. Gramolin, D. Aybas, D. Johnson, J. Adam, and A. O. Sushkov, Search for axion-like dark matter with ferromagnets, Nat. Phys. **17**, 79 (2021).
[34] L. Brouwer *et al.*, Projected sensitivity of DMRadio-m^3: A search for the QCD axion below 1 μeV, Phys. Rev. D **106**, 103008 (2022).
[35] J. Egge *et al.*, First search for dark photon dark matter with a madmax prototype, Phys. Rev. Lett. **134**, 151004 (2025).
[36] A. V. Dixit, S. Chakram, K. He, A. Agrawal, R. K. Naik, D. I. Schuster, and A. Chou, Searching for dark matter with a superconducting qubit, Phys. Rev. Lett. **126**, 141302 (2021).
[37] A. Agrawal, A. V. Dixit, T. Roy, S. Chakram, K. He, R. K. Naik, D. I. Schuster, and A. Chou, Stimulated emission of signal photons from dark matter waves, Phys. Rev. Lett. **132**, 140801 (2024).
[38] K. M. Backes *et al.*, A quantum enhanced search for dark matter axions, Nature (London) **590**, 238 (2021).

[39] P. Zheng *et al.*, Quantum-enhanced dark matter detection using Schrödinger cat states, arXiv:2507.23538.

[40] F. Zhao *et al.*, A Flux-Tunable cavity for dark matter detection, arXiv:2501.06882.

[41] K. Nakazono *et al.*, Search for dark photon dark matter of a mass around 36.1 μeV using a frequency-tunable cavity controlled through a coupled superconducting qubit, arXiv: 2505.15619.

[42] S. Chen, H. Fukuda, T. Inada, T. Moroi, T. Nitta, and T. Sichanugrist, Detecting hidden photon dark matter using the direct excitation of transmon qubits, Phys. Rev. Lett. **131**, 211001 (2023).

[43] S. Chen, H. Fukuda, T. Inada, T. Moroi, T. Nitta, and T. Sichanugrist, Quantum enhancement in dark matter detection with quantum computation, Phys. Rev. Lett. **133**, 021801 (2024).

[44] A. Blais, R.-S. Huang, A. Wallraff, S. M. Girvin, and R. J. Schoelkopf, Cavity quantum electrodynamics for superconducting electrical circuits: An architecture for quantum computation, Phys. Rev. A **69**, 062320 (2004).

[45] A. Blais, A. L. Grimsmo, S. M. Girvin, and A. Wallraff, Circuit quantum electrodynamics, Rev. Mod. Phys. **93**, 025005 (2021).

[46] R. Acharya *et al.*, Suppressing quantum errors by scaling a surface code logical qubit, Nature (London) **614**, 676 (2023).

[47] J. I. Read, The local dark matter density, J. Phys. G **41**, 063101 (2014).

[48] Z. Wang, F. Kong, P. Zhao, Z. Huang, P. Yu, Y. Wang, F. Shi, and J. Du, Picotesla magnetometry of microwave fields with diamond sensors, Sci. Adv. **8**, eabq8158 (2022).

[49] See Supplemental Material at http://link.aps.org/supplemental/10.1103/9p1t-vc9j for the principle, noise analysis, calibration, and details of data process, which includes Refs. [44,50–57].

[50] A. Anferov, S. P. Harvey, F. Wan, Jonathan Simon, and D. I. Schuster, Superconducting qubits above 20 GHz operating over 200 mK, PRX Quantum **5**, 030347 (2024).

[51] A. Anferov, F. Wan, S. P. Harvey, Jonathan Simon, and D. I. Schuster, Millimeter-wave superconducting qubit, PRX Quantum **6**, 020336 (2025).

[52] K. Wurtz, B. M. Brubaker, Y. Jiang, E. P. Ruddy, D. A. Palken, and K. W. Lehnert, Cavity entanglement and state swapping to accelerate the search for axion dark matter, PRX Quantum **2**, 040350 (2021).

[53] Y. Jiang, E. P. Ruddy, K. O. Quinlan, M. Malnou, N. E. Franttini, and K. W. Lehnert, Accelerated weak signal search using mode entanglement and state swapping, PRX Quantum **4**, 020302 (2023).

[54] S. Probst, F. B. Song, P. A. Bushev, A. V. Ustinov, and M. Weides, Efficient and robust analysis of complex scattering data under noise in microwave resonators, Rev. Sci. Instrum. **86**, 024706 (2015).

[55] M. Kudra, J. Biznárová, A. F. Roudsari, J. J. Burnett, D. Niepce, S. Gasparinetti, B. Wickman, and P. Delsing, High quality three-dimensional aluminum microwave cavities, Appl. Phys. Lett. **117**, 070601 (2020).

[56] Y. Tong, L. Wang, W. Zhang, M. Zhu, X. Qin, M. Jiang, X. Rong, and J. Du, A high performance fast-Fourier-transform spectrum analyzer for measuring spin noise spectrums, Chin. Phys. B **29**, 090704 (2020).

[57] R. Kang, M. Jiao, Y. Tong, Y. Liu, Y. Zhong, Y.-F. Cai, J. Zhou, X. Rong, and J. Du, Near-quantum-limited haloscope search for dark-photon dark matter enhanced by a high-Q superconducting cavity, Phys. Rev. D **109**, 095037 (2024).

[58] A. Savitzky and M. J. E. Golay, Smoothing and differentiation of data by simplified least squares procedures, Anal. Chem. **36**, 1627 (1964).

[59] R. Cervantes *et al.*, ADMX-orpheus first search for 70 μeV dark photon dark matter: Detailed design, operations, and analysis, Phys. Rev. D **106**, 102002 (2022).

[60] P. Arias, D. Cadamuro, M. Goodsell, J. Jaeckel, J. Redondo, and A. Ringwald, WISPy cold dark matter, J. Cosmol. Astropart. Phys. 06 (2012) 013.

[61] D. Castelvecchi, IBM releases first-ever 1,000-qubit quantum chip, Nature (London) **624**, 238 (2023).

[62] M. AbuGhanem, IBM quantum computers: Evolution, performance, and future directions, J. Supercomput. **81**, 687 (2025).

[63] A. Megrant *et al.*, Planar superconducting resonators with internal quality factors above one million, Appl. Phys. Lett. **100**, 113510 (2012).

[64] L. Shi *et al.*, Tantalum microwave resonators with ultra-high intrinsic quality factors, Appl. Phys. Lett. **121**, 242601 (2022).

[65] D. P. Lozano *et al.*, Low-loss α-tantalum coplanar waveguide resonators on silicon wafers: fabrication, characterization and surface modification, Mater. Quantum. Technol. **4**, 025801 (2024).

[66] A. P. M. Place *et al.*, New material platform for superconducting transmon qubits with coherence times exceeding 0.3 milliseconds, Nat. Coummn. **12**, 1779 (2021).

[67] C. Wang *et al.*, Towards practical quantum computers: Transmon qubit with a lifetime approaching 0.5 milliseconds, npj Quantum Inf. **8**, 3 (2022).

[68] S. Ganjam *et al.*, Surpassing millisecond coherence in on chip superconducting quantum memories by optimizing materials and circuit design, Nat. Coummn. **15**, 3687 (2024).

[69] O. Dial, D. T. McClure, S. Poletto, G. A. Keefe, M. B. Rothwell, J. M. Gambetta, D. W. Abraham, J. M. Chow, and M. Steffen, Bulk and surface loss in superconducting transmon qubits, Supercond. Sci. Technol. **29**, 044001 (2016).

[70] J. Lisenfeld, A. Bilmes, A. Megrant, R. Barends, J. Kelly, P. Klimov, G. Weiss, J. M. Martinis, and A. V. Ustinov, Electric field spectroscopy of material defects in transmon qubits, npj Quantum Inf. **5**, 105 (2019).

[71] C. A. J. O'Hare, AxionLimits, https://cajohare.github.io/AxionLimits/.